Fibers and Polymers (2023) 24:893–905
https://doi.org/10.1007/s12221-023-00043-9

Online ISSN 1875-0052
Print ISSN 1229-9197

REGULAR ARTICLE

# Fabrication of Acorn-Loaded Chitosan/Gelatin Nanofibrous Web to Increase Antibacterial Activity for Wound-Healing Applications

**Elmira Hadipour-Goudarzi[1] · Nahid hemmatinejad[1] · Mohammad Ali Shokrgozar[2]**

Received: 1 January 2022 / Revised: 21 February 2022 / Accepted: 22 February 2022 / Published online: 6 March 2023


## Abstract

A biocompatible nanofibrous scaffold incorporated with the antibacterial extract of medicinal plant has a synergic effect on the process of wound healing, which is due to its high surface area to volume ratio and mimicking the natural extracellular matrix (ECM) of nanofibrous structure, in addition to lower side effects and antibiotic resistance. Here, biocompatible nanofibers of (chitosan:gelatin)/poly(vinyl alcohol)(PVA) were prepared through electrospinning with acorn extract as a natural cross-linker and antibacterial agent for wound-healing applications. The morphology of nanofibers containing various amounts of acorn extract [0.5%, 1%, and 1.5% (w/v)] was investigated by SEM images. The chemical composition of nanofibers was investigated by FTIR spectra. The tensile testing demonstrated the enhancement of mechanical properties of nanofibrous webs (up to 118% tensile stress, 117% young modulus, and 77% strain at break) by adding acorn extract. The degradation rate and the acorn release rate of cross-linked nanofibers decreased by increasing acorn concentration acting as a natural cross-linker. The release mechanism of cross-linked nanofibers was non-Fickian diffusion for 0.5% acorn loading and Fickian diffusion for 1% and 1.5% acorn loading. The acorn-loaded nanofibers showed a 90% antibacterial activity against *Staphylococcus aureus* bacterium by quantitative standard test method (AATCC 100). Furthermore, the MTT assay showed excellent cell viability and cell attachment of nanofibers for mouse fibroblast (L929) cells. The results indicated that (chitosan:gelatin)/PVA nanofibrous scaffold incorporated with acorn extract was a potent candidate for tissue engineering applications.

**Keywords** Nanofibers · Chitosan · Medicinal plant extract · Antibacterial activity · Wound healing

## 1 Introduction

Nanomaterial is known as a material with at least one dimension ranging from 1 to 100 nm [1, 2]. Three classifications of nanomaterials can be defined based on the number of their nanoscale dimensions including one-dimensional (1D) nano-sized materials such as nanowires and nanorods, two-dimensional (2D) nano-sized materials such as nanofibers, nanoplates, and nanotubes, and three-dimensional (3D) nano-sized materials such as nanoparticles, nanospheres, and quantum dots [3]. Nanomaterial has been used in various fields of applications including biotechnology and agriculture, energy and environment, transportation and aerospace, food and nutrition, textile and clothing, information technology, and healthcare and medicines [3]. The utilization of nanomaterial has been expanded in various parts of medical science such as drug delivery, disease diagnosis, imaging, treatment of cancers, and artificial implants [4]. Nanomaterial in the form of nanofiber which is produced in various profiles (homogeneous nanofiber, coaxial nanofiber, helical and twisted nanofibers, etc.) widely used as an alternative therapeutics for tissue engineering such as bone, cartilage, vascular, cardiac, and skin repairing. [2]. One of the most promising approaches for the engineering of skin tissue scaffolds is using electrospun nanofibers, which provide appropriate biological, mechanical, and physical properties. Some of these properties include absorbing the excess exudate from the wound, the ability to exchange gas and nutrient, acting as a carrier of bioactive materials, and providing protection against microorganism penetration due to the high surface area to volume ratio and the mesh porosities

✉ Nahid hemmatinejad
hemmati@aut.ac.ir

[1] Department of Textile Engineering, Amirkabir University of Technology, Tehran 158754413, Iran

[2] National Cell Bank, Pasteur Institute of Iran, Tehran 1316943551, Iran

[5–7]. Furthermore, the nanofibrous structure mimicking the fibrous component of the natural extracellular matrix (ECM) leads to greater cell compatibility by controlling cellular response including migration, attachment, proliferation, and differentiation, and then more biocompatibility [8, 9]. A wide range of polymers (nature derived and synthetic) have been electrospun alone or in combination for tissue engineering and regenerative medicine [2, 10, 11]. The electrospun nanofibers of chitosan have been widely used in skin tissue engineering [12–16] due to their excellent properties such as biocompatibility, biodegradability, antibacterial, nontoxicity, antifungal, drug loading ability, hemostatic as well as stimulating collagen synthesis, and fibroblast growth factor (FGF) [17–21]. Gelatin is a water-soluble and protein-based polymer derived from acid or alkaline hydrolysis of collagen [20, 22, 23]. It is known to be a promising polymer for tissue engineering and wound-healing applications, because of its biocompatibility, biodegradability, nontoxicity, antigenicity, and high bio-absorptivity [24–26]. Many studies have applied electrospinning of chitosan and gelatin in combination with other polymers or bioactive molecules in tissue engineering [22, 27, 28]. Using medicinal plants for wound-healing applications has been a traditional treatment for decades [29–32]. That is because these plants provide therapeutic effects such as antibacterial, antioxidant, anti-inflammatory, anti-ultraviolet light, antiseptic, anti-wrinkle, and wound-healing stages [29, 33]. Medicinal plant-loaded nanofibrous webs which provide a controlled sustained release within the target site and therefore minimize the side effects as well as mimicking the natural extracellular matrix have received a lot of attention recently [34–36]. An overview of medicinal plant extract-incorporated nanofibrous webs for wound-healing application is presented in Table 1.

The fruit of *Quercus* species, acorn, consists of high content phytochemical compounds, mainly phenolic compounds including phenolic acid, flavonoids, and tannins in addition to carbohydrate, protein, etc. [37]. There are many studies about phytoconstituents and the biological activity of different parts of *Quercus* species (i.e., seed/acorn, bark, and leaves) such as antibacterial [38], antioxidant, anti-inflammatory [39], antifungal, antiviral, wound healing [40, 41], anti-leishmanial [42], and antidiabetic [37]. In this study, the bead-free (chitosan:gelatin)/PVA nanofibers incorporated with acorn extract as a natural antibacterial and cross-linker agent were electrospun for the first time. The morphology, physicochemical, mechanical, and biological properties of nanofibrous webs were characterized and the results suggested that the obtained nanofibers could potentially be used for tissue engineering applications.

## 2 Experimental

### 2.1 Materials

Chitosan (medium molecular weight with 75–85% degree of deacetylation (DD)), gelatin type B from bovine skin, glutaraldehyde (GTA, 25% aqueous solution), and 3-(4,5-dimethyl

**Table 1** Overview of medicinal plant extract incorporated into nanofibers for wound-healing applications

| Polymer/s | Plant | Properties | References |
|---|---|---|---|
| Carboxyethyl Chitosan/PVA and PCL | Chamomile | Antioxidant, antibacterial, cell viability, enhancement of mechanical properties | [43] |
| Chitosan/gelatin/PVA | *Zataria multiflora* | Antimicrobial, nontoxicity, enhancement of mechanical properties | [25] |
| Polylactic acid | *Achillea lycaonica* | Excellent cell compatibility, increase in cell viability, enhancement of mechanical properties | [44] |
| Gelatin/PCL | Aloe vera, hypericum perforatum oil | Decrease in the total oxidant level and oxidative stress index, increase in the tumor necrosis factor-alpha (TNF-α) level | [45] |
| Polycaprolactone, chitosan | Aloe vera | Antibacterial, cell proliferative | [46] |
| Chitosan/gelatin | Cinnamon | Antibacterial, cell attachment and proliferative | [47] |
| Chitosan/PVA | Garlic oil | Antibacterial, increase in liquid absorption, moisture content and mechanical properties | [31] |
| Gelatin | Grape seed polyphenols | Antibacterial, stabilization of silver nanoparticles | [23] |
| Cellulose acetate | Centella asiatica | Increase in water uptake | [48] |
| Chitosan/PLA | Curcumin | Nontoxic activity, antioxidant activity | [49] |
| Gelatin/starch | *Lawsonia inermis* | Fibroblasts attachment, proliferation, collagen secretion, antibacterial | [50] |
| Chitosan/PEO | Green tea | Antibacterial activity, high stability, swelling properties, wound recovery | [51] |
| Poly(4-vinyl pyridine) | Centella asiatica | Promote attachment and proliferation of fibroblasts | [52] |
| Silk fibroin/gelatin | Astragaloside IV | Cell adhesion and proliferation | [53] |

thiazol-2-yl)-2,5-diphenyltetrazolium bromide (MTT) were purchased from Sigma-Aldrich Co., USA. Poly(vinyl alcohol) (PVA) (Mw = 72 kDa) and acetic acid were obtained from Merck Co., Germany. Acorn extract powder (ethanolic extract) with the recovery of solvent was prepared from Jahad Daneshgahi, Tehran, Iran. Mouse fibroblast cells (L929, Cell bank number C161) were obtained from the National Cell Bank, Pasteur Institute, Tehran, Iran.

## 2.2 Solution Preparation

Initially, chitosan (3 wt%) and gelatin (20 wt%) solutions were separately prepared in acetic acid 60% (v/v) by stirring for 24 h and 5 h, respectively, at room temperature. PVA solution (10 wt%) was prepared in distilled water by stirring for 10 h at 50 °C. To prepare (chitosan:gelatin)/PVA solution, the chitosan and gelatin solutions were mixed homogeneously in 50:50 volume ratios and then blended with PVA solution in a 60/40 volume ratio, stirring for 5 h at room temperature. Various amounts of acorn powder [0.5%, 1%, and 1.5% (w/v)] were added to (chitosan:gelatin)/PVA solution and stirred for an additional 12 h to prepare acorn extract-loaded solutions which coded as CGP.0.5, CGP.1 and CGP.1.5, respectively. The (chitosan:gelatin)/PVA solution without acorn extract was also coded as CGP.0.

## 2.3 Electrospinning

The prepared polymer solutions were fed into a 1 ml syringe with a metal capillary needle (23 G) and electrospun on a rotating collector (wrapped with an aluminum foil with a rotating speed of 60 rpm) with the following conditions: 0.2 mL/h feeding rate, 20 kV applied voltage and 14 cm distance between the needle and collector at 25ºC temperature and 30% humidity as shown in Fig. 1. The nanofibrous membranes were cross-linked by GTA vapor (25%) to improve the structural stability and mechanical properties. The samples were placed in the presence of GTA:hydrochloric acid (10:1 v/v) in a sealed glass container heating in an oven for 3 h at 40 °C. To remove any unreacted aldehyde groups from the cross-linked nanofibers, they were washed with glycine (0.2 M) and phosphate-buffered saline (PBS) three times and then dried for 10 h at 30ºC.

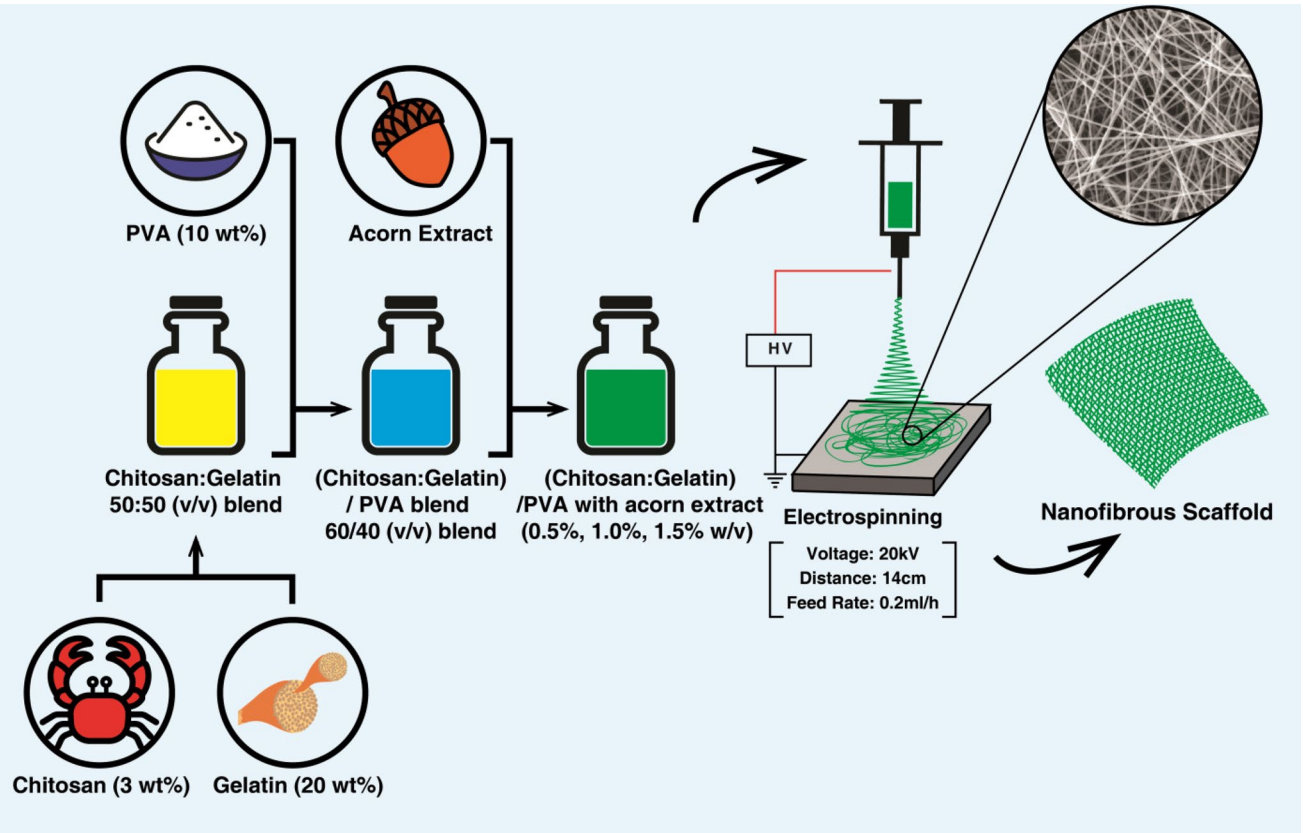


**Fig. 1** The schematic of the preparation of acorn-loaded (chitosan:gelatin)/PVA electrospun nanofibrous web

### 2.4 Total Phenolic Content

The concentration of total phenols of acorn extract was estimated with Folin–Ciocalteau reagent [54]. Suitable aliquots of acorn extract solution or standard tannic acid (12.5, 25, 50, 100, and 200 µg/ml in distilled water) were added to separate flasks. After that, 5 ml of distilled water and 0.5 ml of Folin–Ciocalteu reagent were added and mixed by shaking. After 3 min, 1 ml of sodium carbonate (20%) was added to each flask and diluted with distilled water to 10 ml volume. After 1 h, the absorbance of each sample (in triplicate) was determined against reagent blank at 725 nm using UV–visible spectrophotometer (Human crop, Xma-2000). The amount of total phenolic content was calculated from the calibration curve of tannic acid and expressed as mg of tannic acid equivalent /g of dry acorn extract.

### 2.5 Total Flavonoid Content

The total flavonoid content of acorn extract was measured by the colorimetric method with aluminum chloride [55]. One milliliter of the standard solution of catechine (75, 150, 300, 600, and 1200 µg/ml in methanol) or suitable aliquots of acorn extract solution was added to separate flasks containing 4 ml of distilled water, followed by the addition of 0.3 ml of sodium nitrite (5% w/v). After 5 min, 0.3 ml of aluminum chloride (10% w/v) was added and after 6 min, 2 ml of sodium hydroxide (1 M) was added to each flask and diluted with distilled water to 10 ml volume. The absorbance of the pink color mixture was determined against the water blank at 510 nm. The total flavonoid content was expressed as mg catechin equivalents/g of dry acorn extract. The analysis of each sample was done in triplicate.

### 2.6 Scanning Electron Microscopy (SEM)

The surface morphology of nanofibrous scaffolds was studied with scanning electron microscopy (SEM: Philips XL30 Netherland). The samples were sputter-coated with a thin layer of gold/palladium for 160 s (Sputter coater: Emitech SC7620) to prevent the charging effect. Image analysis software, Image-J (NH, USA) was used to determine the mean diameter and size distribution of nanofibers by measuring the diameter of two individual points of 50 randomly selected nanofibers in each SEM image.

### 2.7 Mechanical Testing

The mechanical properties, including the ultimate tensile strength, elongation at break, and Young's modulus of samples were measured by tensile strength instrument (Instron-5566 universal testing machine) at room temperature. Each nanofibrous web (seven replicates) was cut into a rectangle shape ($5 \times 20$ mm$^2$) and fixed in the middle of the square-shaped paper holder. The holder was clamped and cut at both sides before applying the tensile loading and then exposed to a 50 N load cell in a 5 mm/min extension rate and 20 mm gauge length.

### 2.8 Fourier Transform Infrared Spectroscopy

The Fourier transform infrared (FTIR) spectrometer (Thermo Nicolet, Nexus670, USA) was used to investigate the chemical structure of nanofibrous webs in the spectral range of 500–4000 cm$^{-1}$ (4.0 resolution) at room temperature. The OMNIC software was used to take spectra and collect data from molecular structure and chemical bonds of the samples.

### 2.9 Degradation Analysis

To investigate the stability and physical integrity of nanofibrous scaffolds, their weight loss was measured during the degradation process as follows. The dry samples were carefully weighted (Wi) and then individually immersed in phosphate- buffered saline (PBS, PH 7.4) and incubated at 37 °C for 1, 3, 5, 7, 14, 21, 28, and 35 days. The residual of nanofibrous webs was withdrawn and washed in distilled water two times and then dried and carefully weighted (Wf). The calculated weight loss percentage was reported as an index of their stability according to Eq. (1) [43].

$$\text{Weight degradation}(\%) = \frac{\left(w_i - w_f\right)}{w_i} \times 100. \tag{1}$$

#### 2.9.1 In Vitro Release of Acorn Extract

To study the release profile of acorn extract from nanofibrous scaffolds, $5 \times 5$ cm$^2$ of each sample was carefully weighed and incubated at 37 °C in 6 ml of PBS, as a release media. A certain volume of acorn extract release media was taken out to study the release kinetics and replaced with fresh PBS at certain time intervals. The absorbance of release media was determined by UV–Vis spectrophotometry at each time point (in triplicate) against a blank sample (the release media of nanofibrous web without acorn extract content). The corresponded acorn concentration ($C$) was calculated using the standard graph, according to Eq. (2) which was obtained as follows:

$$\begin{aligned}&\text{Absorbance(at 272 nm)}\\&= 0.02 \times \text{acorn concentration}(\mu\text{g/ml}) - 0.0394.\end{aligned} \tag{2}$$

To plot the standard curve of the acorn extract, the absorbance of five concentrations of acorn extract solution

(in PBS) was characterized against a PBS blank by UV–Vis spectrophotometry (Photonix Ar 2015, Iran) at wavelengths from 200 to 800 nm as shown in Fig. 2. The wavelength of 272 nm was chosen as the characteristic peak of the acorn extract and the standard graph (absorbance vs concentration) of the acorn extract was plotted.

The cumulative release percentage of acorn extract from nanofibrous webs ($E_r$) was calculated according to Eq. (3).

$$E_r(\%) = \frac{V_0 \times C_n + V_r \times \sum_i^{n-1} C_i}{M_{\text{total}}} \times 100, \tag{3}$$

where $V_0$ and $Vr$ are the initial volume of release media and replace media, respectively, $C_n$ is the acorn extract concentration in each media and $m_{\text{total}}$ is the acorn extract contained in each nanofibrous web [43]. To investigate the release kinetics of acorn extract from cross-linked nanofibrous webs, the Korsmeyer–Peppas model was used according to Eq. (4):

$$\frac{M_t}{M_\infty} = K_{KP} t^n, \tag{4}$$

where $M_t/M$ is the release friction at time $t$, $K_{kp}$ is the release velocity constant corresponding to the geometrical and structural characterization of the polymeric system and n is the release exponent in a function of time indicating the release mechanism for $M_t/M_\infty < 0.6$ as follows. If $n \leq 0.45$, the release mechanism is Fickian diffusion, for $0.45 < n < 1$, it is related to anomalous (non-Fickian) diffusion, and for $n = 1$ and $n > 1$, it is related to the case II transport (zero-order release) and super case II transport mechanism release, respectively [11, 56, 57].

## 2.10 Antibacterial Activity Test

The antibacterial activity of samples was evaluated against Gram-negative bacteria, *Escherichia coli* (*E. coli:* ATCC 25,922), and Gram-positive bacteria, *Staphylococcus aureus* (*S. aureus:* ATCC 6538), through quantitative standard test method (AATCC 100). The *E. coli* and *S. aureus* bacteria were grown separately, in nutrient broth (37 °C for 18 h). Bacterial cells were collected by centrifugation (3000×*g* for 15 min), washed with PBS three times, and then resuspended in PBS and diluted to an approximate bacterial concentration of $1 \times 10^5$ CFU/ml. Each sample (in triplicate) was cut in a circular shape (5 cm diameter), placed in distinct Petri dishes, and sterilized with UV radiation (30 min each side). A certain volume of bacterial suspension was added to each sample and then incubated at 37 °C overnight. For recovering viable bacterial cells, 20 ml of sterile PBS was added to each sample and vortexed vigorously for 5 min. Serial dilutions of 1:10 ratio were prepared from each test in duplicate. A volume of 0.1 ml of dilutions was spread onto nutrient and incubated at 37 °C for 16–18 h. The bacterial count for each sample was calculated, and the antibacterial activity was calculated according to Eq. (5) [18].

$$R = \frac{(B - A)}{B} \times 100, \tag{5}$$

where $R$ is the bacterial reduction percentage, and $A$ and $B$ are the initial number and recovered count of bacteria, respectively.

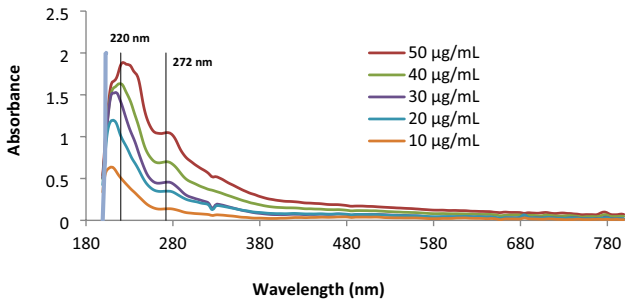


**Fig. 2** The absorbance of five concentrations of acorn extract dissolved in PBS against PBS blank at wavelengths from 200 to 800 nm

## 2.11 Cytotoxicity and Cell Growth

To investigate the viability, cell growth, and proliferation of the nanofibrous webs, the quantitative determination method, 3-(4,5-dimethyl thiazol-2-yl)-2,5-diphenyltetrazolium bromide assay (MTT), was done according to standard ISO 10993-5 (indirect contact) using the mouse fibroblast (L929) cells as follows. Firstly, the L929 (NCBI C161) were defreezed and then put in Roswell Park Memorial Institute (RPMI) medium with 10% (v/v) fetal bovine serum (FBS) and incubated in air containing 90% humidity and 5% $CO_2$ at 37 °C, replacing the culture medium every 3–4 days. The samples (1.5 $cm^2$) with four replicates were washed with ethanol 70% (v/v) for 5 min and then sterilized with UV radiation (1 h each side). The sterile samples were placed in a 12-well plate and then cells at a density of $5 \times 10^3$ L929 cells (with 100 µl culture medium) were added to each well and incubated (37 °C) for 4 h. After ensuring cell adherence, a certain amount of culture medium was added to each well and thrown completely away after 1, 3, and 7 days. 400 µl of MTT formazan solution was added to each and incubated for 4 h. The absorbance of each sample was detected by spectrophotometer (BioTek ELx808, USA) at 570 nm as optical density (OD). The viability percentage of each sample normalized by the control group (nanofibrous web without acorn extract) was calculated according to Eq. (6).

$$\text{Viability}(\%) = \frac{\text{mean OD of the sample}}{\text{mean OD of control}} \times 100. \tag{6}$$

### 2.12 Visualization of Cell Attachment

The morphology of cells cultured on the surface of nanofibrous scaffolds was observed by SEM after 24 h cell seeding. The sterile samples were placed in a 24-well plate and then cells at a density of $3 \times 10^4$ L929 (with 100 µl of culture medium) were added and incubated for 5 h. A certain amount of culture medium with FBS 10% was added to each well and removed after 24 h by washing with PBS for 30 s. The samples were treated with GTA 3.5% to fix the cells and washed with deionized water and a series of ethanol solutions (50%, 60%, 70%, 80%, and 96%). Finally, the dried samples were imaged with SEM.

### 2.13 Statistical Analysis

All of the experimental data were collected in triplicate and the results were presented as average ± standard deviation (SD). Statistical analysis as an analyzing way to evaluate variance and independent samples were used with one-way ANOVA at $p < 0.05$ statistical significance.

## 3 Results and Discussion

### 3.1 Morphology of Nanofibrous Webs

The SEM images, mean diameter, and diameter distribution histograms of (Cs:Ge)/PVA nanofibers incorporated with various amounts of acorn extract are shown in Fig. 3. The mean diameter of (chitosan:gelatin)/PVA nanofiber increased from 120.53 to 142.97 nm, 185.81 nm, and 215.24 nm by adding 0.5%, 1%, and 1.5% of acorn extract, respectively. Adding acorn extract led to an increase in the molecular entanglements between chitosan, gelatin, and PVA polymers and acorn extract, as a natural cross-linker. It caused an increase in the viscosity and repulsive force to stretch the solution droplet in the Taylor cone phase and, consequently, an increase in the mean diameter of nanofibers. Zhang et al. indicated the C–N interactions created between the natural phenolic compound and the amino group in the gelatin structure [58].

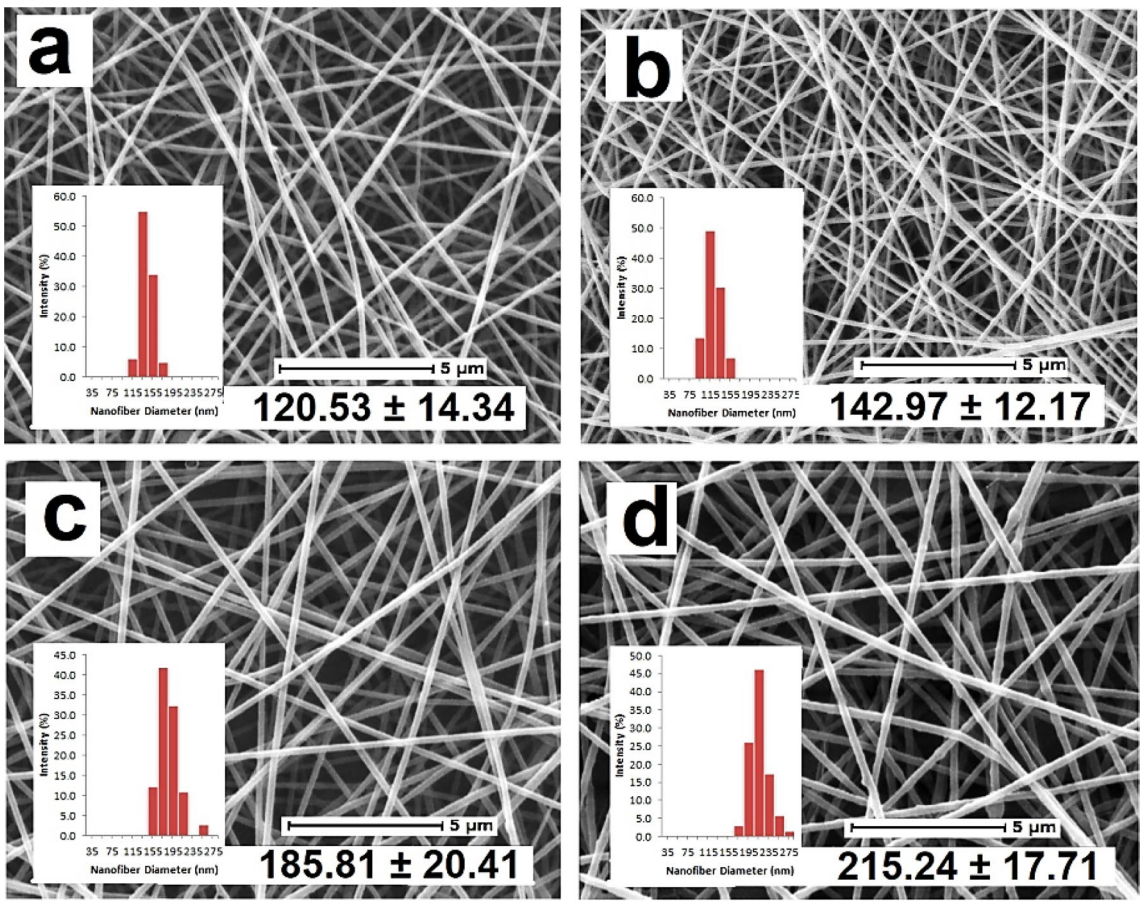


**Fig. 3** The SEM images, mean diameter and diameter distribution histograms of **a** CGP.0, **b** CGP.0.5, **c** CGP.1 and **d** CGP.1.5 nanofibrous webs

### 3.2 Total Phenolics and Flavonoids

The results revealed that the acorn extract consists of a high content of total phenol (805.50 ± 76.90 mg of tannic acid equivalents/g dry acorn extract) and total flavonoids (189.07 ± 5.39 mg of catechin equivalents/g dry acorn extract). Many studies investigating the phytochemical compounds of acorn indicated that the main and ubiquitous compounds of acorn were phenolic acid, flavonoid, and tannins [37, 59].

### 3.3 FTIR Spectroscopy

The FTIR spectra of chitosan, gelatin, PVA, and acorn extract powders, in addition to the FTIR spectra of CGP.0 and CGP.1 nanofibrous webs, before and after cross-linking with GTA vapor, are illustrated in Fig. 4. The FTIR spectrum of gelatin powder exhibits a peak at 3414 $cm^{-1}$ attributed to stretching of the OH and NH groups (amide A). The characteristic peaks at 1635 $cm^{-1}$, 1560 $cm^{-1}$, and 1240 $cm^{-1}$ are associated with amide I (C=O), amide II (N–H and C–H), and amide III (C–N stretch and N–H in the phase bending), respectively [25, 60]. The FTIR spectrum of chitosan powder displays a characteristic peak at 3427 $cm^{-1}$ related to N–H and O–H stretching and intermolecular hydrogen bonding of the chitosan backbone [18]. The absorbance peaks at 1656 $cm^{-1}$, 1590 $cm^{-1}$, and 1074 $cm^{-1}$ are attributed to amide I (C=O), amide II ($NH_2$ bending), and C–O stretching, respectively [25, 61]. Other peaks at 1431 $cm^{-1}$ and 1319 $cm^{-1}$ are associated with $CH_3$ symmetrical deformation modes [24]. Moreover, the peaks at around 900 $cm^{-1}$ to 1153 $cm^{-1}$ are assigned to the saccharine structure of chitosan [24]. The FTIR spectrum of PVA powder shows the characteristic peaks at 3424 $cm^{-1}$, 2924 $cm^{-1}$, 1435 $cm^{-1}$, and 1098 $cm^{-1}$ assigned to O–H stretching vibration, $CH_2$, CHOH, and CO groups, respectively [25, 35, 62]. The FTIR spectrum of acorn extract displays an absorbance peak at 3401 $cm^{-1}$ related to phenolic groups and a large amount of intermolecular and intramolecular hydrogen bonding in its structure. The peaks at 1611 $cm^{-1}$, 1522 $cm^{-1}$, and 1444 $cm^{-1}$ are related to stretching C=C vibration from the aromatic rings [63]. Furthermore, the peaks at 1706 $cm^{-1}$, 1200 $cm^{-1}$, 1330 $cm^{-1}$, and 1030 $cm^{-1}$ are assigned to C=O, C–OH symmetrical and asymmetrical C–O vibrations, respectively. The peaks around 680–860 $cm^{-1}$ are attributed to the CH bond vibration in the benzene rings [25, 60]. Furthermore, the FTIR spectrum of the CGP.0 nanofibers (before cross-linking with GTA) exhibits an absorbance peak at 3347 $cm^{-1}$ associated with NH and OH stretching vibration and intermolecular and intramolecular hydrogen bondings. Furthermore, the obvious sharp peaks at 2938 $cm^{-1}$, 1654 $cm^{-1}$, and 1540 $cm^{-1}$ are related to C–H bonding, amide I (C=O), and amide II (N–H), respectively [18, 25]. Therefore, the CGP.0 nanofibrous web is composed of all three polymers, including chitosan, gelatin, and PVA [18]. The peak at 3347 $cm^{-1}$ from the FTIR spectrum of CGP.0 nanofibers (before cross-linking with GTA) is shifted gradually to higher wavenumber 3365 $cm^{-1}$ for CGP.1 (before cross-linking with GTA), which indicates the increase of intermolecular hydrogen bonding between the polymers and phenolic groups of acorn extract content, as a natural cross-linker [64–66]. Furthermore, the relative intensity of peaks around 680–860 $cm^{-1}$ ascribed to the CH bond of aromatic groups is higher in CGP.1 nanofibers (before cross-linking with GTA), compared to CGP.0 nanofibers (before cross-linking with GTA), which could exhibit the existence of acorn extract in its structure [60]. Moreover, the FTIR spectra from CGP.0 and CGP.1 nanofibers, which are cross-linked with GTA, exhibit broader and more intense peaks at 3415 $cm^{-1}$ and 3426 $cm^{-1}$ wavenumbers, respectively, in comparison with non-cross-linked ones. It could correspond to hydrogen bonding between GTA and nanofibers contents [65]. Moreover, there are two new peaks at 960 $cm^{-1}$ and 870 $cm^{-1}$ in cross-linked nanofibrous scaffold corresponding to symmetric and asymmetric vibration of COCOC groups [61].

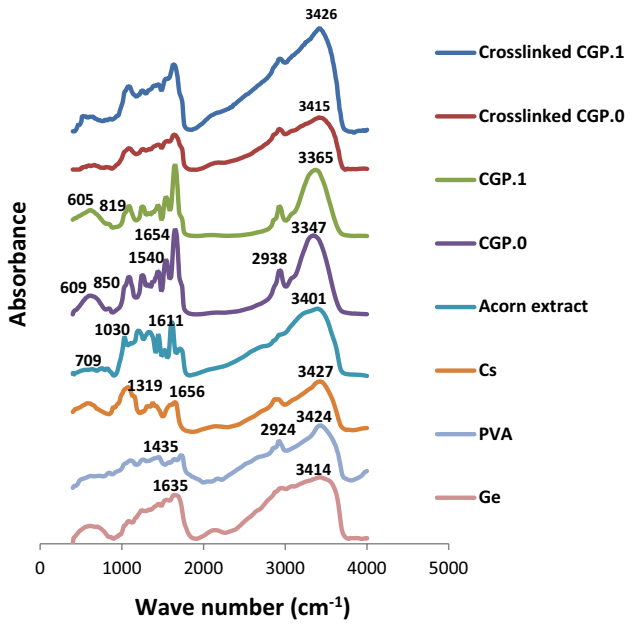


**Fig. 4** The FTIR spectra of chitosan, gelatin, PVA, and acorn powders and CGP.0 and CGP.1 nanofibrous webs, before and after cross-linking with GTA vapor

### 3.4 Mechanical Properties

One of the critical factors for preparing a skin wound dress is achieving appropriate mechanical properties to withstand

handling, stretching, and physiological forces during the wound-healing processes. The values of ultimate tensile stress (UTS), elongation to break (EB), and Young's modulus (EM) of non-cross-linked and cross-linked CGP.0, CGP.0.5, CGP.1, and CGP.1.5 nanofibrous webs are indicated in Table 2. The UTS and EM of cross-linked nanofibers increased and their EB decreased by introducing new bondings within cross-linked nanofibers, which caused to reduce the slippage of nanofibers and improve the mechanical properties of the nanofibrous web [25, 67]. Reui-Yi Tsai et al. revealed that cross-linking of chitosan/gelatin/PVA nanofibers by GTA vapor enhanced the UTS and decreased the EB of nanofibrous webs because of polymer chain restrictions [22]. The UTS of CGP.0.5, CGP.1 and CGP.1.5 nanofibers increase by 87%, 96%, and 118%, respectively, as well as their EM increase by 43%, 50%, and 117%, respectively. These were attributed to introduction of intermolecular interactions between the phenolic compounds of acorn extract (acting as a cross-linker) and polymeric structure of nanofibrous webs, such as C–N covalent bonds and hydrogen bonding, which caused an increase in stretch resistance and tensile strength [58]. The role of tannic acid as an effective cross-linker of gelatin film on the increase of tensile strength was proved [60, 66]. Adding acorn extract led to an increase in the diameter of the nanofibers and then reduced the number of contact points and frictional cohesion forces between nanofibers, which resulted in the enhancement of the EB of CGP.0.5 and CGP.1 nanofibrous webs to 50% and 77%, respectively [68]. However, by adding more acorn extract (1.5%), the hydrogen bond force between polymer and acorn extract overcomes the lower number of contact points (because of higher nanofiber diameter) between nanofibers, which resulted in greater resistance to elongation and higher rigidity.

### 3.5 Biodegradation Analysis

One of the critical factors for a biocompatible scaffold is the proportion between scaffold biodegradation and tissue repair rate [69]. To investigate the physical stability of cross-linked nanofibrous webs, the weight loss percentages of cross-linked CGP.0, CGP.0.5, CGP.1, and CGP.1.5 nanofibrous scaffolds were obtained at 1, 3, 5, 7, 14, 21, 28, and 35 days (Fig. 5). The weight loss of all samples increased suddenly and then continued with a gradual and constant slope as shown in Fig. 5. The highest weight loss rate was attributed to CGP.0 with 38% mass loss, which decreased by 34%, 14%, and 12% by adding 0.5%, 1%, and 1.5% of the acorn extract, respectively. It might be due to the effect of the acorn extract as a cross-linking agent, which caused intermolecular reactions between its phenolic compounds and polymers [22, 58, 60, 65]. Bitao Lu et al. indicated that the interactions between the phenolic hydroxyls and the hydrogen bond of gelatin acted as a cross-linking agent for chitosan/gelatin sponges [66]. Moreover, the mean diameter of nanofibrous webs increased by adding acorn extract content, leading to the decrease in the surface area to volume ratio and then decrease in their connection with the surrounding aquatic medium and, consequently, structural degradation [43].

### 3.6 In Vitro Release Study of Acorn Extract

The cumulative release percentages of cross-linked CGP.0.5, CGP.1, and CGP.1.5 nanofibrous webs (in triplicate) incubated (37 °C) in PBS solution for 1, 3, 5, 7, 14, 21, and 28 days are plotted in Fig. 6. There was a sudden release on day 1 of about 19%, 15%, and 7%, attributed to acorn extract release from CGP.0.5, CGP.1, and CGP.1.5, respectively. The release rate increased gradually until day 7 and then continued with a relatively constant rate untile day 28,

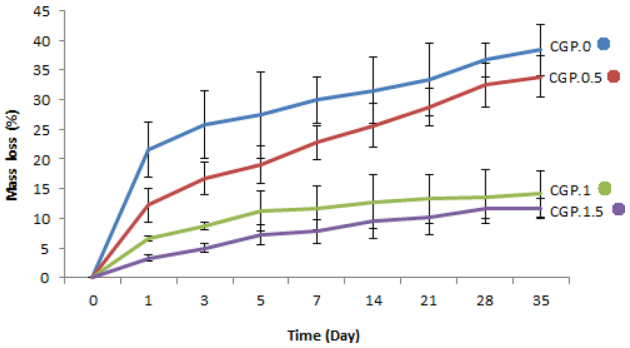


**Fig. 5** The weight loss percentage of cross-linked CGP.0, CGP.0.5, CGP.1, and CGP.1.5 nanofibrous webs

**Table 2** The mechanical properties of nanofibrous webs before and after cross-linking

| Test | Samples | CGP.0 | CGP.0.5 | CGP.1 | CGP.1.5 |
|---|---|---|---|---|---|
| Ultimate tensile stress (MPa) | Non-cross-linked | 1.90 | 2.61 | 3.19 | 3.38 |
| | Cross-linked | 3.45 | 6.45 | 6.75 | 7.52 |
| Strain at break (%) | Non-cross-linked | 8.54 | 9.79 | 17.5 | 3.54 |
| | Cross-linked | 4.58 | 6.88 | 8.12 | 3.96 |
| Young's modululs (MPa) | Non-cross-linked | 86.01 | 127.33 | 165.35 | 146.7 |
| | Cross-linked | 147.17 | 209.66 | 220.71 | 319.81 |

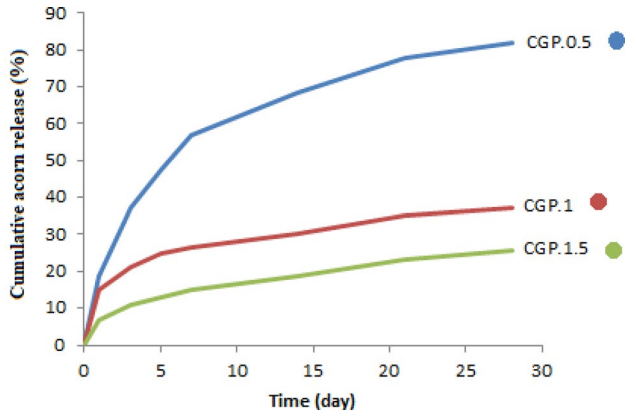


**Fig. 6** The cumulative acorn release (%) from cross-linked CGP.0.5, CGP.1, and CGP.1.5 nanofibrous webs

as shown in Fig. 6. The release from the biodegradable polymeric system was governed by two main factors, including desorption/diffusion of acorn extract and dissolution/erosion of the polymeric system [70]. The sudden release was concerned with the amount of acorn extract content in the nanofibrous structure located on the surface of nanofibers, which were in more contact with an aqueous environment [43, 70]. Moreover, filling the existing pores in the nanofibrous structure and its swelling led to passing the dissolved acorn extract through the pores and entering the surrounding media. This was followed by the gradual increase in the decomposition of the polymeric system and as a result the release of the trapped acorn extract in the nanofibrous structure [70]. The final release rate of acorn extract from CGP.0.5, CGP.1, and CGP.1.5 reached 82%, 37%, and 26% respectively, which reduced despite the increase of the acorn extract content. It might be due to the higher structural stability of nanofibrous webs in the presence of acorn extract as a cross-linker agent by increasing hydrogen bonding between them as shown in Fig. 5 [58, 60, 64]. Moreover, the mean diameter of nanofibrous webs arose by increasing the acorn extract content, which led to the lower surface area to volume ratio and then reduction in the surface contact with the surrounding environment [71]. The Korsmeyer–Peppas kinetic model was used to investigate the mechanism of acorn extract release from nanofibrous webs. The n value, as release exponent, indicates the release mechanisms for $M_t/M_\infty < 0.6$. The release velocity constant ($K_{kp}$ value) and regression coefficient ($R^2$) were calculated for CGP.0.5, CGP.1, and CGP.1.5, which are summarized in Table 3. The n values of CGP.1 and CGP.1.5 (for $M_t/M_\infty < 0.6$, within 28 days) were equal to 0.27 and $0.39 < 0.45$, respectively, located in the Fickian diffusion category, and $n$ value equal to $0.57 > 0.45$ for CGP.0.5 (for $M_t/M_\infty = 0.57 < 0.6$ within 7 days) corresponded to non-Fickian diffusion, which related to drug diffusion and polymer swelling together [56, 57].

### 3.7 Antibacterial Activity Test

The results of antibacterial activity (AATCC 100 standard test method) of CGP.1 and CGP.0 nanofibrous scaffold (after cross-linking with GTA), against Gram-negative bacteria, *E. coli*, and Gram-positive bacteria, *S. aureus,* are illustrated in Fig. 7. The antibacterial percentage of (chitosan:gelatin)/PVA nanofibrous scaffolds without acorn extract was 40% ($6 \times 10^4$ CFU/ml[1]) against *S. aureus.* The antibacterial activity of chitosan has been investigated by many authors and has been attributed to some mechanisms, including the interactions between the negative charge of the bacterial cell membrane and positive charge of polycationic chitosan molecules, which cause cell membrane disruption of bacteria and leaking intracellular contents [14, 16]. Moreover, the antibacterial activity of acorn extract has been reported in many studies, because of bioactive compounds such as flavonoids, tannins, polyphenols, and alkaloids [37]. The mechanism of phenolic toxicity to microorganisms was assigned to the ability of hydroxyl groups or phenolic compounds, which founded in acorn extract to complex with protein and bacterial cell wall polypeptides, which caused decomposite of the mitochondrial and cell membrane of bacteria, and therefore change its permeability and death of bacterial cell [30, 72, 73]. It could be the reason of high antibacterial activity of acorn-loaded nanofibers (CGP.1) against S. aureus (90% reduction in bacterial concentration, $1 \times 10^4$ CFU.ml$^{-1}$). Moreover, many studies indicate that the multilayer structure of Gram-negative bacterium cell, enveloped with an outer membrane containing lipopolysaccharide, leads to more resistance against antimicrobial agents rather than Gram-positive bacteria [63, 74]. This could be the reason for the less than 5% ($9.5 \times 10^4$ CFU/ml) and 10% ($9 \times 10^4$ CFU/ml) antibacterial activity of CGP.0 and CGP.1 against gram-negative bacteria, *E. coli.*

**Table 3** The kinetics of acorn release in Korsmayer–Peppas mathematic model

| Samples code | $n$ | $K_{KP}$ | $R^2$ |
|---|---|---|---|
| CGP.0.5 | 0.56527 ± 0.0257 | 19.1957 ± 1.0077 | 0.9960 ± 0.0039 |
| CGP.1 | 0.2659 ± 0.0032 | 15.5193 ± 1.7321 | 0.9910 ± 0.0014 |
| CGP.1.5 | 0.3892 ± 0.0013 | 6.8631 ± 0.94 | 0.9964 ± 0.0011 |

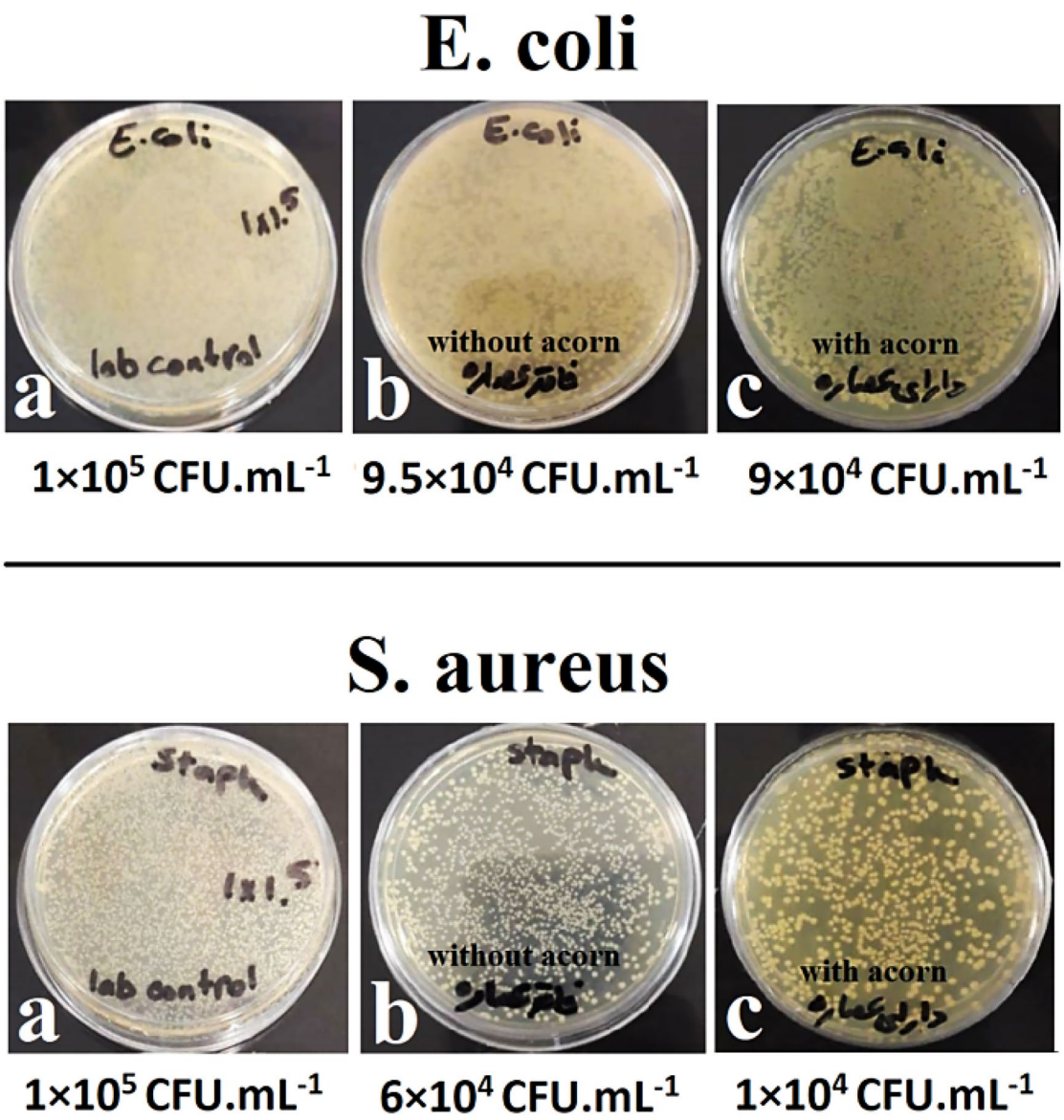


**Fig. 7** The antibacterial activity of nanofibrous webs against *E. coli* (up) and *S. aureus* (down) according to ATCC 100 method. **a** Laboratory control at the initial bacterial concentration ($1 \times 10^5$ CFU/ml), **b** and **c** the bacterial concentration of CGP.0 and CGP.1, respectively

### 3.8 Cytotoxicity and Cell Growth

The biocompatibility of nbanofibers with various amounts of acorn extract was evaluated with MTT assay in vitro. This method is based on changing yellow tetrazolium dye powder to insoluble dark purple formazan crystals, which only occur in living cells. The intensity of optical density has a direct relationship with formazan concentration and the number of living cells as a consequence. The viability and optical density of CGP.0, CGP.0.5, CGP.1, and CGP.1.5 nanofibrous scaffolds after 1, 3, and 7 days of culturing time are illustrated in Fig. 8. The viability of the nanofibers grew by adding acorn extract and keeping for 1, 3, and 7 days, which was confirmed by the gradual enhancement of their optical density [37] as shown in Fig. 8. It is consistent with the result of Bitao Lu et al., which revealed that the incorporation of chitosan/gelatin sponge with tannin as a cross-linker had no toxicity against L929 fibroblast cell and promoted wound healing in vivo [40, 66]. Yin et al. have shown that the phenolic compounds isolated from *Quercus mongolica* Fisch. ex Ledeb had a significant effect on inhibition of inflammatory cytokines and chemokines as well as expression of immune factors, thereby having potential for inflammatory skin diseases reduction [75, 76].

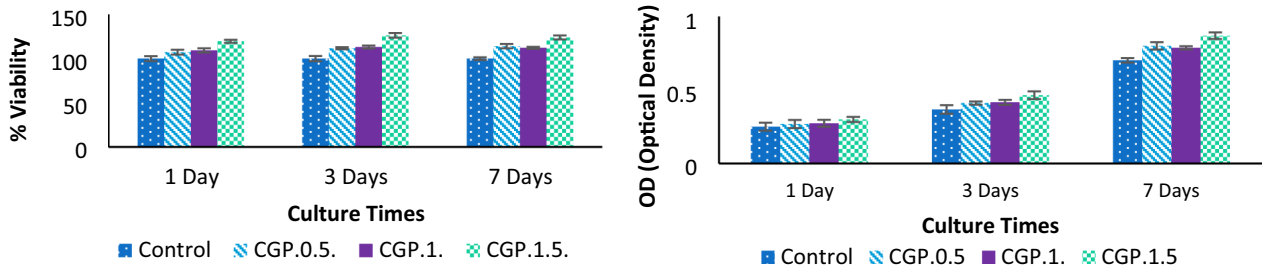


**Fig. 8** The viability of CGP.0, CGP.0.5, CGP.1, and CGP.1.5 nanofibrous webs after 7 days of cell culturing compared with control (100% viability) (left) and their optical density on adding acorn and over a period of time (right)

### 3.9 Morphology of the Cells

The SEM images of the cell morphology of CGP.0, CGP.0.5, CGP.1, and CGP.1.5 after 24 h of culturing are illustrated (three magnifications) in Fig. 9. The cell attachment, anchoring to nanofibrous scaffolds, spreading, and interconnections between L929 cells were observed for all the samples which increased by adding acorn extract. It could confirm the biocompatibility of the nanofibrous scaffold, not only because of their natural compositions and the efficient role of acorn extract combined with chitosan and gelatin, but also because of their nanofibrous structure with high surface area to volume ratio mimicking an ECM structure [37, 77, 78]. Xu et al. revealed that the ternary composite nanofiber of tannic acid/chitosan/pullulan favored the growth and attachment of fibroblast cells [79].

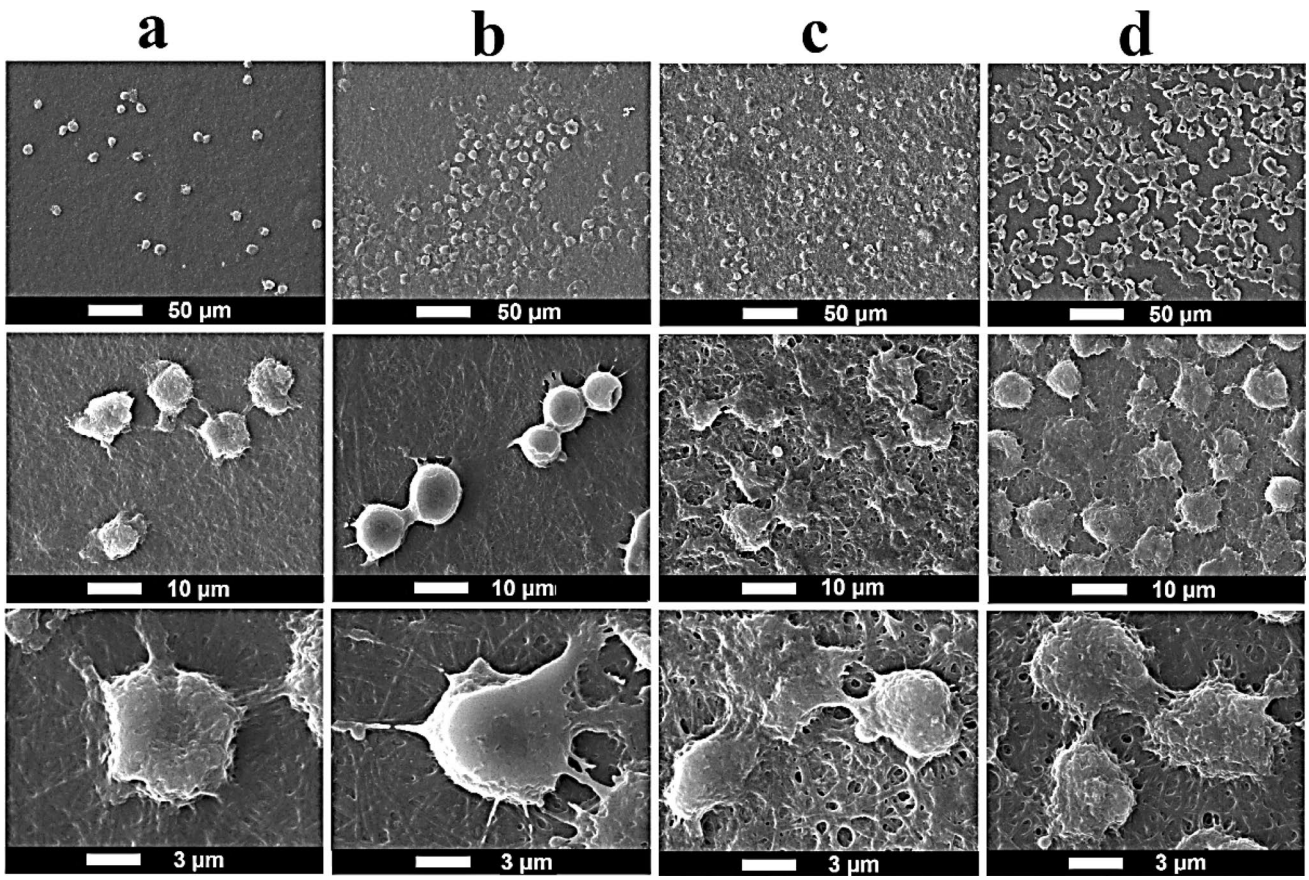


**Fig. 9** The SEM images of L929 cells attachment on the surface of **a** CGP.0, **b** CGP.0.5, **c** CGP.1, and **d** CGP.1.5 nanofibrous webs after 24 h cell seeding

## 4 Conclusion

The nanofibrous composite of (chitosan:gelatin)/PVA incorporated with acorn extract was successfully electrospun for wound-healing applications with lower side effects like antibiotic resistance. Cross-linking of nanofibrous scaffolds with GTA vapor led to improving their mechanical properties. The mechanical properties and physical stability of nanofibrous webs are dramatically enhanced by increasing acorn concentration while increasing the nanofiber diameter. The acorn release rate of nanofibers decreased despite the increase in acorn content. This release followed two mechanisms including non-Fickian diffusion for CGP.0.5 and Fickian diffusion for CGP.1 and CGP.1.5. The acorn extract-loaded nanofibrous webs showed excellent antibacterial activity (90%) against *S. aureus*, according to AATCC 100 standard. The results showed that acorn-loaded nanofibers had no toxicity against L929 fibroblast cells. In conclusion, acorn extract-loaded (chitosan:gelatin)/PVA nanofiber showed excellent biocompatibility for skin tissue engineering, not only because of its natural biocompatible composition, but also because of its nanofibrous structure with high surface area to volume ratio and mimicking the natural ECM.

**Acknowledgements** The authors appreciate the National Cell Bank of Iran, Pasteur Institute of Iran, for cytocompatibility tests as well as the Microbiology and Biotechnology Lab, University of Tehran, Iran, for the antibacterial test.

**Data availability** Data will be available upon contacting the corresponding author.

### Declarations

**Conflict of Interest** All authors declare that they have no conflict of interest.

## References

1. N.A. Singh, Environ. Chem. Lett **15**, 185–191 (2017)
2. A.D. Juncos-Bombin, N.J. Dunne, H.O. McCarthy, Mater. Sci. Eng. C **114**, 110994 (2020)
3. T. Hassan, A. Salam, A. Khan, S.U. Khan, H. Khanzada, M. Wasim, M.Q. Khan, I.S. Kim, J. Polym. Res **28**, 1–22 (2021)
4. G. Nikaeen, S. Abbaszadeh, S. Yousefinejad, Nanomedicine **15**, 1501–1512 (2020)
5. S. Homaeigohar, A.R. Boccaccini, Acta Biomater. **107**, 25–49 (2020)
6. M. Mirjalili, S. Zohoori, J. Nanostruct. Chem **6**, 207–213 (2016)
7. D.M. Ibrahim, A. Kakarougkas, N.K. Allam, Mater. Today Chem **5**, 11–23 (2017)
8. S. Hinderer, S.L. Layland, K. Schenke-Layland, Adv. Drug Deliv. Rev **97**, 260–269 (2016)
9. S. Du, N. Zhou, Y. Gao, G. Xie, H. Du, H. Jiang, L. Zhang, J. Tao, J. Zhu, Nano Res. **13**, 2525–2533 (2020)
10. D. Sundaramurthi, U.M. Krishnan, S. Sethuraman, Polym. Rev. **54**, 348–376 (2014)
11. R.S. Ambekar, B. Kandasubramanian, Eur. Polym. J **117**, 304–336 (2019)
12. I. Bano, M. Arshad, T. Yasin, M.A. Ghauri, M. Younus, Int. J. Biol. Macromol. **102**, 380–383 (2017)
13. R.A.A. Muzzarelli, Carbohydr. Polym **76**, 167–182 (2009)
14. F. Croisier, C. Jérôme, Eur. Polym. J **49**, 780–792 (2013)
15. M.Z. Elsabee, H.F. Naguib, R.E. Morsi, Mater. Sci. Eng. C **32**, 1711–1726 (2012)
16. T. Dai, M. Tanaka, Y.Y. Huang, M.R. Hamblin, Expert Rev. Anti. Infect. Ther. **9**, 857–879 (2011)
17. L. Tan, J. Hu, H. Huang, J. Han, H. Hu, Int. J. Biol. Macromol **79**, 469–476 (2015)
18. E. Hadipour-Goudarzi, M. Montazer, M. Latifi, A.A.G. Aghaji, Carbohydr. Polym. **113**, 231–239 (2014)
19. A. Moeini, P. Pedram, P. Makvandi, M. Malinconico, G. Gomez d'Ayala, Carbohydr. Polym. **233**, 115839 (2020)
20. J. Jacob, J.T. Haponiuk, S. Thomas, S. Gopi, Mater. Today Chem. **9**, 43–55 (2018)
21. L. Behbood, S. Karimi, E. Mirzaei, G. Mohammadi, M. Azami, E. Arkan, Fibers Polym. **19**, 1454–1462 (2018)
22. R.Y. Tsai, S.C. Hung, J.Y. Lai, D.M. Wang, H.J. Hsieh, J. Taiwan Inst. Chem. Eng. **45**, 1975–1981 (2014)
23. X. Han, Z. Xing, S. Si, Y. Yao, Q. Zhang, Fibers Polym. **15**, 2572–2580 (2014)
24. H.H. Sokker, A.M. Abdel Ghaffar, Y.H. Gad, A.S. Aly, Carbohydr. Polym. **75**, 222–229 (2009)
25. N.T. Ardekani, M. Khorram, K. Zomorodian, S. Yazdanpanah, H. Veisi, H. Veisi, Int. J. Biol. Macromol. **125**, 743–750 (2019)
26. E. Mohamed, A. Fitzgerald, T. Tsuzuki, Mater. Today NANO **16**, 100137 (2021)
27. J. Jafari, S.H. Emami, A. Samadikuchaksaraei, M.A. Bahar, F. Gorjipour, Biomed. Mater. Eng. **21**, 99–112 (2011)
28. M. Pezeshki-Modaress, M. Zandi, S. Rajabi, Prog. Biomater. **7**, 207–218 (2018)
29. U. Das, S.S. Behera, S. Singh, S.I. Rizvi, A.K. Singh, Phyther. Res. **30**, 1895–1904 (2016)
30. M.M. Cowan, Clin. Microbiol. Rev. **12**, 564–582 (1999)
31. R. Zhang, M. Lei, B. Hu, H. Tu, M. Hu, Fibers Polym. **0**, 1–9 (2021)
32. B.P. Nagori, R. Solanki, Res. J. Med. Plant **5**, 392–405 (2011)
33. Y.P. Talekar, K.G. Apte, S.V. Paygude, P.R. Tondare, P.B. Parab, J. Ayurveda Integr. Med. **8**, 73–81 (2017)
34. A. Zarghami, M. Irani, A. Mostafazadeh, M. Golpour, A. Heidarinasab, I. Haririan, Fibers Polym **16**, 1201–1212 (2015)
35. K. Lee, S. Lee, Fibers Polym. **21**, 999–1012 (2020)
36. G. Jin, M.P. Prabhakaran, D. Kai, S.K. Annamalai, K.D. Arunachalam, S. Ramakrishna, Biomaterials **34**, 724–734 (2013)
37. E. Burlacu, A. Nisca, C. Tanase, Forests **11**, 1–24 (2020)
38. D.F. Basri, S.H. Fan, Indian J. Pharmacol. **37**, 26–29 (2005)
39. B. George, N. Bhatia, T.V. Suchithra, Eur. Polym. J. **157**, 110640 (2021)
40. J. Chokpaisarn, S. Chusri, T. Amnuaikit, W. Udomuksorn, S.P. Voravuthikunchai, PeerJ **2017**, 1–16 (2017)
41. R. Thakur, N. Jain, R. Pathak, S.S. Sandhu, Evid.-Based Complement. Altern. Med **2011**, 1–17 (2011)
42. A. Farghi-Yamchi, M. Dabirzadeh, Y. Maroufi, Med. Lab. J **12**, 23–28 (2018)
43. M. Shokrollahi, S.H. Bahrami, M.H. Nazarpak, A. Solouk, Int. J. Biol. Macromol. **147**, 547–559 (2020)
44. M. Emin, S. Cesur, T. Taskin, G. Erdemir, D. Serap, Y. Muge, L. Kabasakal, O. Gunduz, Eur. Polym. J. **120**, 109239 (2019)
45. Z. Guleken, J. Depciuch, H. Ege, G. İlbay, C. Kalkandelen, D. Ozbeyli, H. Bulut, G. Sener, N. Tarhan, S. Erdem Kuruca,

Spectrochim. Acta Part A Mol. Biomol. Spectrosc. **254**, 119639 (2021)
46. J. Yin, L. Xu, Int. J. Biol. Macromol. **160**, 352–363 (2020)
47. S. Ahmadi, A. Hivechi, S.H. Bahrami, P.B. Milan, S.S. Ashraf, Int. J. Biol. Macromol. **173**, 580–590 (2021)
48. N. Barnthip, A. Muakngam, J. Bionanosci. **8**, 313–318 (2014)
49. B. Dhurai, N. Saraswathy, R. Maheswaran, P. Sethupathi, P. Vanitha, S. Vigneshwaran, V. Rameshbabu, Front. Mater. Sci **7**, 350–361 (2013)
50. Z. Hadisi, J. Nourmohammadi, S.M. Nassiri, Int. J. Biol. Macromol **107**, 2008–2019 (2018)
51. M. Sadri, S. Arab-Sorkhi, H. Vatani, A. Bagheri-Pebdeni, Fibers Polym. **16**, 1742–1750 (2015)
52. I.A. Isoglu, N. Koc, Fibers Polym. **21**, 1453–1465 (2020)
53. Y.H. Shan, L.H. Peng, X. Liu, X. Chen, J. Xiong, J.Q. Gao, Int. J. Pharm. **479**, 291–301 (2015)
54. S. Kamtekar, V. Keer, V. Patil, J. Appl. Pharm. Sci **4**, 61–65 (2014)
55. K.M. Yoo, C.H. Lee, H. Lee, B.K. Moon, C.Y. Lee, Food Chem. **106**, 929–936 (2008)
56. R.W. Korsmeyer, R. Gurny, E. Doelker, P. Buri, N.A. Peppas, Int. J. Pharm. **15**, 25–35 (1983)
57. S. Dash, P.N. Murthy, L. Nath, P. Chowdhury, Acta Pol. Pharm. Drug Res. **67**, 217–223 (2010)
58. X. Zhang, M.D. Do, P. Casey, A. Sulistio, G.G. Qiao, L. Lundin, P. Lillford, S. Kosaraju, Biomacromol **11**, 1125–1132 (2010)
59. A.F. Vinha, J.C.M. Barreira, I.C.F.R. Ferreira, M.B.P.P. Oliveira, Ref. Ser. Phytochem, 273–287 (2020)
60. M.L.L.R. do Menezes, N.R. da Pires, P.L.R. da Cunha, M. de Freitas-Rosa, B.W.S. de Souza, J.P.A. de Feitosa, M.S.M. de Souza-Filho, Food Packag. Shelf Life **19**, 7–15 (2019)
61. S. Gomes, G. Rodrigues, G. Martins, C. Henriques, J.C. Silva, Int. J. Biol. Macromol. **102**, 1174–1185 (2017)
62. L. Fan, H. Yang, J. Yang, M. Peng, J. Hu, Carbohydr. Polym. **146**, 427–434 (2016)
63. Z. Kharat, M. Sadri, M. Kabiri, Fibers Polym. **22**, 989–999 (2021)
64. N. Cai, C. Li, C. Han, X. Luo, L. Shen, Y. Xue, F. Yu, Appl. Surf. Sci. **369**, 492–500 (2016)
65. Y.N. Chen, C. Jiao, Y. Zhao, J. Zhang, H. Wang, ACS Omega **3**, 11788–11795 (2018)
66. B. Lu, T. Wang, Z. Li, F. Dai, L. Lv, F. Tang, K. Yu, J. Liu, G. Lan, Int. J. Biol. Macromol. **82**, 884–891 (2016)
67. K. Jalaja, D. Naskar, S.C. Kundu, N.R. James, Carbohydr. Polym. **136**, 1098–1107 (2016)
68. M. ElMessiry, N. Fadel, Alex. Eng. J **58**, 885–890 (2019)
69. T. Agarwal, R. Narayan, S. Maji, S. Behera, S. Kulanthaivel, T.K. Maiti, I. Banerjee, K. Pal, S. Giri, Int. J. Biol. Macromol. **93**, 1499–1506 (2016)
70. M. Sadri, A. Mohammadi, H. Hosseini, Nanomed. Res. J **1**, 112–121 (2016)
71. A.M. Moydeen, M.S. Ali-Padusha, E.F. Aboelfetoh, S.S. Al-Deyab, M.H. El-Newehy, Int. J. Biol. Macromol. **116**, 1250–1259 (2018)
72. E. Aleebrahim-Dehkordy, M. Rafieian-kopaei, H. Amini-Khoei, S. Abbasi, J. Diet. Suppl. **16**, 408–416 (2019)
73. I.J. Sagbo, A.J. Afolayan, G. Bradley, Asian Pac. J Trop. Biomed. **7**, 817–825 (2017)
74. T.J. Silhavy, D. Kahne, S. Walker, Cold Spring Harb. Perspect. Biol. **2**, a000414 (2010)
75. S. Ghuman, B. Ncube, J.F. Finnie, L.J. McGaw, E. Mfotie Njoya, R.M. Coopoosamy, J. Van Staden, South Afr. J. Bot. **126**, 232–240 (2019)
76. J. Yin, H.H. Kim, I.H. Hwang, D.H. Kim, M.W. Lee, Molecules **24**, 3094 (2019)
77. S. Ranganathan, K. Balagangadharan, N. Selvamurugan, Int. J. Biol. Macromol. **133**, 354–364 (2019)
78. X. Wang, B. Ding, B. Li, Mater. Today **16**, 229–241 (2013)
79. F. Xu, B. Weng, R. Gilkerson, L.A. Materon, K. Lozano, Carbohydr. Polym. **115**, 16–24 (2015)